



Bubble formation and evolution behavior from vertical wall orifice

Zhao-Wei Ma^{1,2} · Xiao-Ling Wu^{1,2} · Qin Zhang^{1,2} · Guo Yang^{1,2} · Gui-Min Liu¹ · Hua Li¹ · Wei Liu¹

Received: 18 December 2018 / Revised: 28 September 2019 / Accepted: 1 October 2019 / Published online: 21 November 2019
© China Science Publishing & Media Ltd. (Science Press), Shanghai Institute of Applied Physics, the Chinese Academy of Sciences, Chinese Nuclear Society and Springer Nature Singapore Pte Ltd. 2019

Abstract Bubble formation is an integral part of the two-phase flow science. Through numerical simulation and experiments using different air flow rates and orifice diameters, the present study aims at investigating the behavior of bubble formation and evolution from vertical wall orifice in quiescent pure water. For the experiments, the images of the bubble formation process under different working conditions were recorded using a high-speed camera and analyzed the entire process. The bubble formation process can be divided into three stages, namely nucleation, stable growth, and necking. According to the obtained results, bubble forms only when the air-phase pressure exceeds the threshold pressure at wall orifice. Due to the influence of the threshold pressure and buoyancy, the bubble volume decreases with an increase in the wall orifice diameter for the same flow rate. Moreover, the volume of fluid method is applied to simulate bubble formation in a three-dimensional model and the “buffer volume” is considered in the simulation model. The simulation results

matched well with the experimental data, which proves the existence of threshold pressure and the periodic pressure fluctuation at the wall orifice.

Keywords Bubble formation · Vertical wall orifice · Threshold pressure · Pressure fluctuation

1 Introduction

As a key component in the degassing system of thorium molten salt reactor, the main function of a venturi-type bubble generator is to produce bubbles that are uniform in their size [1–3]. Bubble behavior in a generator can be divided into three processes, namely bubble formation, bubble movement, and bubble fragmentation. The study of the formation and detachment of bubbles is one of the most important processes to describe and predict the behavior of bubbles in a bubble generator. In recent decades, several kinds of bubble column reactors have been widely studied and applied in various fields due to their favorable characteristics in terms of sufficient inter-phase contact and mixing, high mass and heat transfer rates, uniform concentration, and temperature distributions [4–9]. The size of the gas bubbles, an important parameter that influences the performance of the bubble column reactor, determines the bubble rising velocity and gas residence time. It, also, in turn governs the gas holdup, the interfacial area, and, subsequently, the gas–liquid mass transfer rate. More significantly, the interaction between the bubbles, such as the coalescence and fracture of the bubbles, can change the mass transfer area between the phases [10].

Several scientists and engineers have conducted numerous researches using experimental and

This work was supported by the Strategic Priority Research Program of the Chinese Academy of Sciences (No. XDA0202000) and the National Natural Science Foundation of China (No. 11535009).

✉ Gui-Min Liu
liuguimin@sinap.ac.cn

✉ Hua Li
lihua@sinap.ac.cn

✉ Wei Liu
liuwei@sinap.ac.cn

¹ Shanghai Institute of Applied Physics, Chinese Academy of Sciences, Shanghai 201800, China

² University of Chinese Academy of Sciences, Beijing 100049, China

computational fluid dynamics (CFD) methods to study bubble formation and detachment behavior [11–18]. Pourtousi et al. used the volume of fluid (VOF) method within the ANSYS Fluent commercial code to simulate the two-dimensional methane bubble formation and rise from the orifice at the bottom wall. The simulation results were consistent with the experimental results for bubble formation [11]. Bhunia et al. conducted a study on bubble formation from a single nozzle in a coflowing liquid configuration. The described theoretical model predicts the bubble diameter at detachment and is in good agreement with the experimental results [16]. Nahra et al. conducted a study on bubble formation and detachment from wall orifice. They found that bubble formation and detachment can be classified into two stages called the expansion stage and detachment stage. They also determined the bubble formation and detachment process based on the rate of gravity, air inlet diameter, and inlet and fluid velocity; however, in their experiments, the air intake direction was consistent with that of buoyancy [17, 18]. In recent years, many studies have been conducted on bubble formation and detachment from a micro-orifice at the bottom wall surface [19–22]. Xie et al. [20] studied bubble formation in a bubble column reactor with an orifice plate of 0.054–0.5 mm in diameter. The results showed that the evolution of the bubble formation process can be described using three or four stages for different orifices. Two important concepts called “threshold pressure” and “wait time” were first proposed in their study. Zhang et al. [21] investigated the bubble dynamic behavior at the submerged micron orifice. The outcome indicated that the bubble formation process can be divided into three stages, namely nucleation, stable growth, and necking. In most of the previous studies, the gas was injected into the liquid through the bottom wall orifice or intake pipe; hence, the air inlet direction was similar to the buoyancy of the bubble. In these studies, bubbles were approximately spherical or axial symmetric as there was no lateral wall effect. However, the bubbles formed in the vertical wall orifice were not spherical or axisymmetric, and the lateral wall effect played an important role in bubble formation, detachment, and rising [23]. Zhang et al. used two-dimensional (2D) CFD-VOF model to numerically analyze the rising bubbles in the side channel. The results showed that the bubbles would stick to the wall during the rising process. Zhao et al. conducted a similar study with a three-dimensional (3D) CFD-VOF model and obtained identical results. The contact angle played a dominant role in their model [24, 25]. Cai et al. used the VOF method to study the process of bubble formation and detachment from a vertical wall orifice of a venturi-type bubble generator in a cross-flowing liquid. They found that the pressure fluctuation and mass flow rate should be considered to have an

essential impact on bubble formation and detachment; however, the calculated results failed to predict the reflux phenomenon shown in the experiment [26].

A bubble generator may be used in the vertical state of the degassing system of molten salt reactor and other applications. However, bubble formation from the vertical wall orifice has hardly been studied, primarily due to research difficulty and the key point in the study of bubble generation from the wall orifice. The purpose of this study is to investigate the behavior of bubble formation and evolution from vertical wall in quiescent pure water. Instant images of bubble motion are recorded using a high-speed photographic technique. With a digital image processing technique, parameters such as bubble size, the spatial evolution of bubble shape, and the changes of velocities with different height, can be obtained. The variations and relationship among these parameters under different working conditions are discussed. The numerical simulation of bubble formation under different conditions is also carried out with buffer volume using the VOF model.

2 Experimental system and Numerical methods

2.1 Experimental setup

The experimental setup used in this study is outlined in Fig. 1. It is composed of a gas supply system, bubble generator system, and measurement system. The gas supply system is made up of pure standard air cylinder, air flowmeter with a range of 0–100 mL/min (Sevenstar, CS200), and a computer. Experiments were carried out in a vertically placed transparent Plexiglas tank (360 mm height, $90 \times 90 \text{ mm}^2$ interior cross-sectional area) with

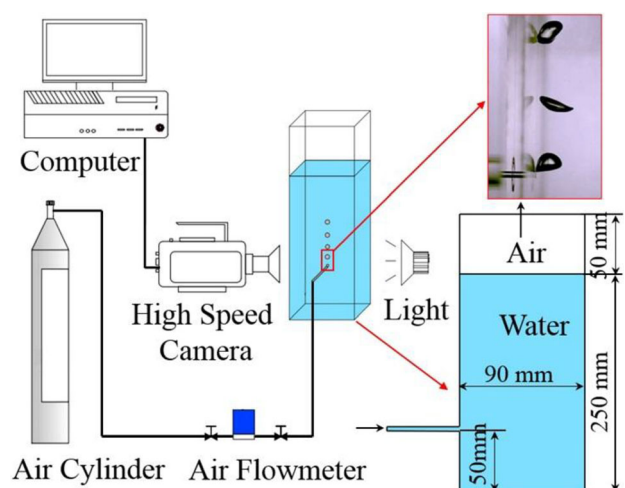


Fig. 1 (Color online) The schematic of experimental setup

three different sizes of wall orifice (1.0 mm, 1.5 mm, and 2.0 mm). The experiment began after the tank was filled with the quiescent pure water up to 200 mm above the top edge of the wall orifice. The measurement system is composed of a Photron-type high-speed camera (Vision Research, v1210), LED light source, and computer. The LED panel light is settled on the right-hand side of the tank, and the camera is placed on the opposite side to record the evolution process of bubbles, including the shape of bubbles, time of bubble formation, and detachment process. In this experiment, high-speed camera recorded images at a frame rate of 10000 frame/s and resolution of 640×768 pixel were used with $1.16 \mu\text{s}$ as the exposure time. Finally, the bubble images were processed and analyzed.

The densities of deionized water and pure air, which are used as the main working medium, are 998.2 kg/m^3 and 1.204 kg/m^3 , respectively. The experimental conditions are listed in Table 1.

The bubble formation period and bubble formation time are defined as follows:

1. Bubble formation period T : The time between the start of the formation of one bubble and the next bubble.
2. Bubble formation time t : The time between the start of the formation of one bubble and the start of the detachment of that bubble.

2.2 Governing equations

The bubble formation simulation in a bubble column reactor has been studied using the VOF method. This method has been used in several studies to investigate the interaction of gas and liquid interfaces, particularly in bubble formations [22, 27]. In the VOF model, a single set of momentum equations is shared by the fluids, and the volume fraction of each of the fluids in each computational cell is tracked throughout the domain. The VOF method utilizes the volume ratio function F :

$$F = \frac{\text{Volume of fluid in unit}}{\text{Volume of unit}}, \quad (1)$$

$$F = \begin{cases} 0 & \text{in bubbles} \\ 0 < F < 1 & \text{interface} \\ 1 & \text{in liquid fluid} \end{cases}. \quad (2)$$

The volume fraction of the fluid in the flow field is calculated using the following transport equation:

$$\frac{\partial F}{\partial t} + \nabla \cdot (F \vec{v}) = 0. \quad (3)$$

As the pressure and Reynolds number are small in the flow field, laminar flow and incompressible calculation method are used for calculation. The Navier–Stokes equations are given by:

$$\nabla \cdot \vec{v} = 0, \quad (4)$$

$$\frac{\partial(\rho \vec{v})}{\partial t} + \nabla(\rho \vec{v} \vec{v}) = -\nabla p + \nabla[\mu(\nabla \vec{v} + \nabla \vec{v}^T)] + \vec{F}_s + \rho \vec{g}. \quad (5)$$

where v is the velocity of the mixture, ρ is the density of two-phase flow, t is the time, F_s is the volumetric forces, p is the pressure, g is the gravity, and μ is the viscosity.

The contact angle is related to the properties of gas, liquid, and solid phases. In particular, when air bubbles form from the vertical wall orifice, the contact angle has a strong influence on the bubble formation process. The contact angle between the transparent Plexiglas and bubble was measured in the laboratory, and it was found to be 68° .

2.3 Numerical method

According to Mukundarkrishnan et al. when the distance from the wall to the bubble exceeds three times the bubble diameter, the effect of the sidewalls can be ignored [23]. In the experiment, the maximum bubble diameter was less than 8 mm, and so the physical model of the simulation process was simplified to a three-dimensional model with a cross section of $32 \times 32 \text{ mm}^2$ and height of 50 mm. The geometric model for this experiment is shown in Fig. 2. In the experiment, it was found that the formation time and period of bubbles were related to the volume size of the inlet pipe between the air flowmeter and wall orifice, which was 0.012 ml. This part of the volume is defined as the buffer volume and simplified by calculation as shown on the left-hand side of Fig. 2.

Firstly, the preprocessing of numerical calculation was conducted including the establishment of geometric model, partition grid, and boundary conditions. Next, the grid independence verification was performed. ANSYS Fluent 16.0 was used for simulation calculation. Based on the

Table 1 Experimental conditions

Parameters	Numeric value or name
Medium	Deionized water and air
Density (water) (kg/m^3)	998.2
Density (air) (kg/m^3)	1.204
Wall orifice diameter (D_N) (mm)	1.0, 1.5, 2.0
Air flow rate (mL/min)	20, 40, 60, 80, 100
Temperature ($^\circ$)	20

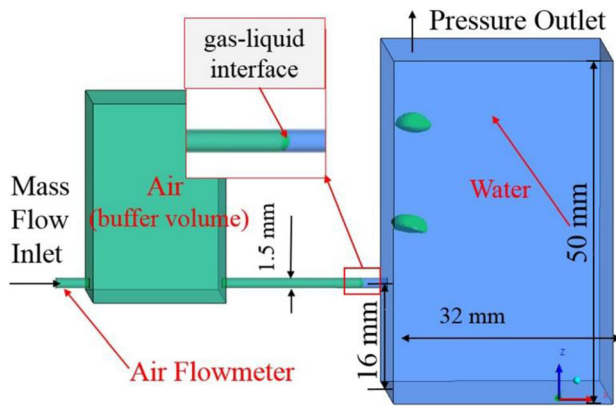


Fig. 2 (Color online) Computational model and boundary conditions

simulation results for different grid sizes, the model with 1717130 grid number was selected for calculation. A transient model based on an explicit scheme with a time step of 0.00001 s and Courant number 0.25 was used. The inlet and outlet boundary conditions were defined as mass flow inlet and pressure outlet, respectively. All the solid walls were considered to have no-slip boundary condition, and the contact angle was approximately 68° .

3 Results and Discussion

The dimensionless time t^* is defined as t/t_0 . Therefore, in Fig. 3, $t^* = 1$ indicates that the bubbles are at the end of the detachment.

3.1 Bubble formation process

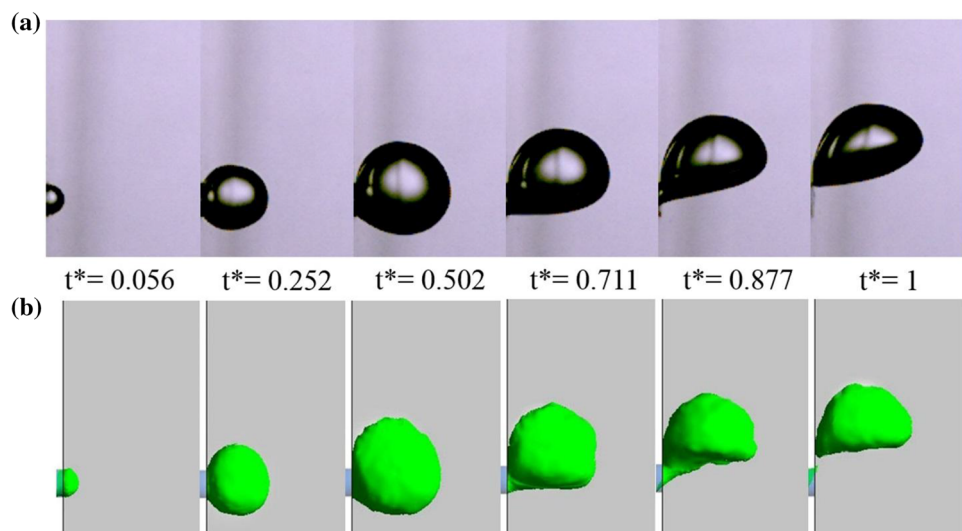
To reflect the bubble formation process and the size of the bubble formation more intuitively, the bubble size,

bubble formation time t , and bubble formation period T are selected. These three parameters are discussed based on the size of the orifice diameter and air flow rate. Zhang et al. [21] found that the bubble dynamic behavior at the submerged micron orifice can be divided into three stages, namely nucleation, stable growth, and necking. Figure 3a shows the formation process of air bubbles with an orifice of 1.5 mm in diameter and air flow rate of 40 mL/min. The bubble formation process from vertical wall orifice can also be divided into the following three stages:

- Nucleation stage ($t^* \leq 0.056$):** Bubbles begin to grow when air is injected into the tank. In this stage, bubbles are small and the surface tension is much greater than buoyancy. Thus, the surface tension dominates the entire stage. Once the bubble cap diameter is equal to the orifice diameter, the surface tension reaches its maximum value. However, the time period of this stage is quite short.
- Stable growth stage ($0.056 < t^* \leq 0.711$):** As the volume of the bubbles increases, the effect of buoyancy becomes more apparent in the formation of bubbles. Under the effect of buoyancy, the bubble begins to shape into a cap.
- Necking stage ($0.711 < t^* \leq 1$):** After the bubbles volume increases to a certain extent, the bubbles continue to move upward and the gas-liquid interface begins to fall off from the bottom of the orifice, which is the biggest difference from the bubble formation process by the bottom wall orifice. Eventually, the bubbles completely fall off from the wall orifice.

The schematic diagram of the forces acting on the growing bubble at vertical wall orifice is shown in Fig. 4. Here, the wall orifice is D_N . The contact angle of the bubble is α and β due to asymmetrical growth.

Fig. 3 (Color online) Bubble formation process ($D_N = 1.5$ mm, air flow rate = 40 mL/min):
a experimental results and
b calculation results



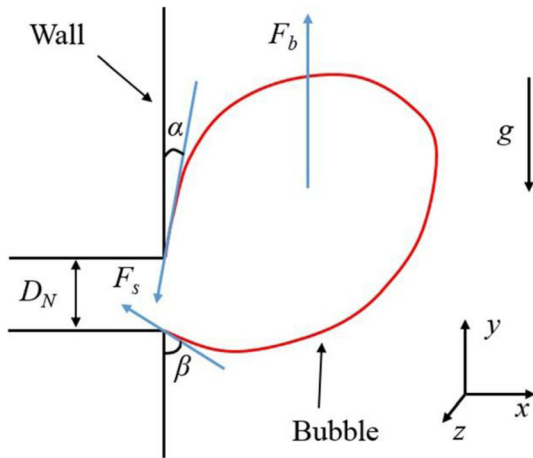


Fig. 4 (Color online) The main forces acting on the bubble

The forces acting on the bubble in the x and y directions are given by the following equations:

$$\sum F_x = F_{sx} + F_{dux} + F_{cp} = \frac{d(mU_{cx})}{dt}, \tag{6a}$$

$$\sum F_y = F_{sy} + F_{duy} + F_b = \frac{d(mU_{cy})}{dt}, \tag{6b}$$

where F_{sx} and F_{sy} are the x and y surface tension, respectively. F_{dux} and F_{duy} are bubble growth forces caused by asymmetric growth and inertial forces, respectively. F_{cp} is the contact pressure accounting for the fact that the bubble is in contact with a solid wall rather than being completely surrounded by a liquid. F_b is the buoyancy force. The surface tension force is given by the following equations [28, 29]:

$$F_{sx} = -\frac{1}{2}D_N\sigma \int_0^{2\pi} \sin \gamma d\phi, \tag{7a}$$

$$F_{sy} = -\frac{1}{2}D_N\sigma \int_0^{2\pi} \cos \gamma \cos \phi d\phi, \tag{7b}$$

where ϕ is the polar angle around the bubble and

$$\gamma = \gamma(\phi) \approx \alpha + (\beta - \alpha) \frac{\phi}{\pi} \tag{8}$$

Equation (8) is substituted in Eqs. (7a) and (7b) and simplified as follows:

$$F_{sx} \approx -D_N\sigma \frac{\pi}{\beta - \alpha} (\cos \alpha - \cos \beta), \tag{9a}$$

$$F_{sy} \approx -1.25D_N\sigma \frac{\pi(\beta - \alpha)}{\pi^2 - (\beta - \alpha)^2} (\sin \beta + \sin \alpha). \tag{9b}$$

As $\beta \rightarrow \alpha$,

$$F_{sx} \approx -D_N\sigma\pi \sin \beta, \tag{10a}$$

$$F_{sy} \approx -2.5D_N\sigma(\beta - \alpha) \frac{\sin \beta}{\pi}. \tag{10b}$$

The buoyancy force is denoted as follows:

$$F_b = (\rho_l - \rho_g)V_Bg. \tag{11}$$

To understand the formation process of bubbles, the forces on the y -axis are discussed as follows: (A) In the initial stage of bubble formation, the bubble is symmetric with respect to the central axis, and thus, $\alpha = \beta$. According to Eq. (10b), the surface force in the y direction is 0. The volume of the bubble is quite small, and at this stage, the buoyancy of the bubble is negligible. The maximum surface tension is reached when the bubble diameter is equal to the orifice diameter. As the volume of the bubble increases, the force F_{duy} is negligible relative to the buoyancy. (B) When the wall orifice diameter D_N is 1.5 mm, the range of F_{sy} is calculated based on Eq. (9b) using MATLAB. When $0 < \alpha < \pi/2$ and $0 < \beta < \pi/2$, the surface force in the y direction is less than 9.0×10^{-5} N. When the buoyancy force is 9.0×10^{-5} N, the bubble radius is approximately 1.3 mm based on Eq. (11). It is, thus, clear that the upward buoyancy force F_b is greater than the surface tension force F_{sy} , and the bubble begins to move upward and deform a cap. (C) When β is greater than $\pi/2$, the buoyancy acting on the bubble is more significant due to the continuous growth in the bubble volume. The gas–liquid interface begins to fall off from the bottom of the orifice, and eventually, the bubbles completely fall off from the wall orifice.

3.2 Bubble size and liquid reflux

Figure 5 shows the images of the bubbles at the moment of detachment recorded by a high-speed camera under different wall orifice diameters and air flow rates. Accordingly, the size of bubble formation is noticeably related to the orifice diameter and air flow rate. Based on this, the following conclusions are drawn, as shown in Fig. 6a and b: (1) Within a certain range, the smaller the orifice diameter, the larger would be the bubble volume. This result is contrary to that of bubble formation from bottom wall orifice [21]. (2) For the same orifice diameter, the volume of bubbles increases as the air flow rate increases. The results can be preliminarily explained as shown in Fig. 6c. For the same air flow rate, the smaller the orifice diameter, the longer would be the bubble formation period (T). Therefore, the bubble volume will be larger if the period of bubble formation is longer. It can also be concluded that the bubble formation period decreases with an increase in the air flow rate for the same orifice diameter, indicating that the speed of bubble formation is faster. However, the following results are obtained when the relationship between the bubble formation time and other parameters is further studied, as shown in Fig. 6d. With the

Fig. 5 (Color online) Bubbles detachment moment under different wall orifice diameters and air flow rates

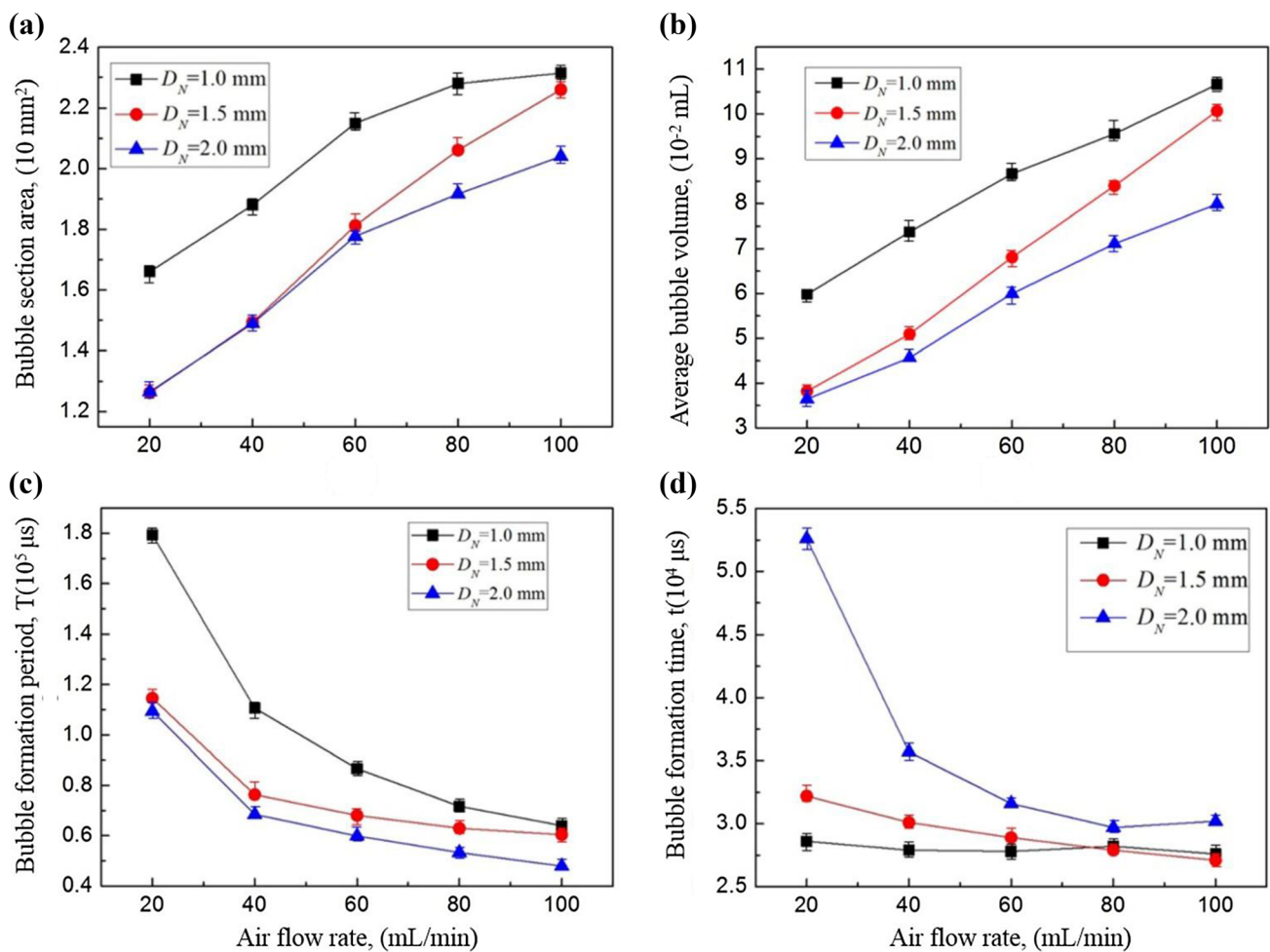
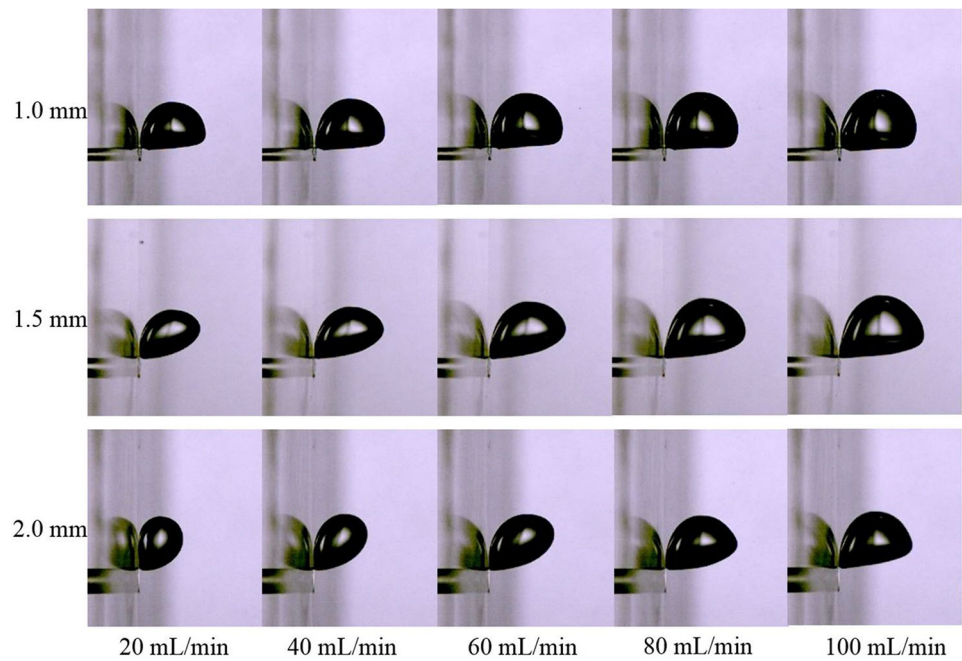


Fig. 6 (Color online) The relationship between bubble parameter and the air flow rate under different orifice diameters: **a** bubble section area, **b** average bubble volume, **c** bubble formation period, and **d** bubble formation time

same air flow rate, the smaller the air orifice diameter is, the shorter would be the bubble formation time (t). However, it is clear from the above discussion that the smaller the orifice diameter is, the larger would be the bubble volume when it falls off. This is because although the air flow rate is the same, the instantaneous rate of air entering the bubble through the wall orifice is different due to different wall orifice diameters. However, in the case of bottom wall orifice, bubble volume increases with an increase in the orifice diameter for the same flow rate [11, 20, 21]. This could be the result of wall effect and buoyancy.

The above results are mainly caused by the surface tension in the air inlet pipe. In other words, the different orifice diameters have different threshold pressures during the bubble formation process [20]. The different threshold pressures decrease the size of the bubbles with an increase in the orifice diameter.

The effect of surface tension in the wall orifice is denoted as follows:

$$\Delta p = \frac{4\sigma}{D_N}, \quad (12)$$

where Δp is the pressure difference in the gas and liquid phase, which is the required threshold pressure when the bubble formation begins.

It can be noted from Eq. (12) that the smaller the orifice diameter, the larger is the pressure threshold. When D_N is small, a higher pressure is required. Once the threshold is reached, the gas quickly enters the bubble. Therefore, the gas has greater instantaneous velocity. In other words, the gas entering the bubble has greater inertial force and momentum flux force. This leads to more gas entering the bubble, making it bigger. Due to the greater inertial force and momentum flux force, bubbles quickly form, grow, and

fall off at the wall orifice. Figure 7 shows the evolution process of the height of bubble center at different times when the wall orifice diameter is 1.0, 1.5, and 2.0 mm, respectively, and the air flow rate is 40 mL/min. Based on the results, it can be concluded that the larger the orifice diameter, the longer will be the bubble formation time. Thus, the time of the buoyancy effect before the bubble falls off will increase, central height of the bubble will be higher, and shape of the bubble will be stretched in the direction of buoyancy.

After the bubble falls off, the air pressure in the inlet pipe reduces. Under the effect of surface tension, the liquid will flow back into the air inlet pipe. The bubble will form again when the air pressure in the inlet pipe reaches the critical pressure; thus, the pressure in the air inlet pipe fluctuates. Further related explanation is provided in the later sections through calculations.

3.3 Simulation of the bubbles formation process

The calculated results are in good agreement with the experimental results. Figure 3b shows the evolution of bubble formation and detachment by calculating a three-dimensional model with orifice diameter of 1.5 mm and air flow rate of 40 mL/min. According to the statistical analysis for this condition, the calculated average volume of the bubble is 4.87×10^{-2} mL, and the average volume of the bubble in the experiment is 4.93×10^{-2} mL. It is determined that the ratio of the calculated bubble volume to the measured bubble volume is 0.988. Thus, the error is found to be 1.2%. Simultaneously, the bubble formation period is calculated to be approximately 0.074 s. In this condition, the bubble formation period measured by the experiment is 0.074 s. Table 2 shows the specific calculation results with an orifice diameter of 1.5 mm.

The above results show that the computational model can properly simulate the formation and detachment of bubbles on the vertical wall orifice. Meanwhile, the calculated results can accurately predict the liquid reflux phenomenon in the experiment. However, the calculation model used in the literature does not provide this result and has a continuous bubble generation process [26]. Therefore, it is necessary to add buffer volume into the calculation model.

Figure 8 is a schematic diagram of the relationship between pressure and dimensionless time ($T^* = T/T$) in the wall orifice. It can be seen that the pressure on the wall orifice increases rapidly as the bubbles begin to form. The maximum critical pressure, which is the threshold pressure, can be reached in a short time. At this point, the bubble diameter is equal to the orifice diameter. Afterward, the pressure on the wall orifice rapidly drops. This is because once the bubble begins to grow, the velocity of the air flow

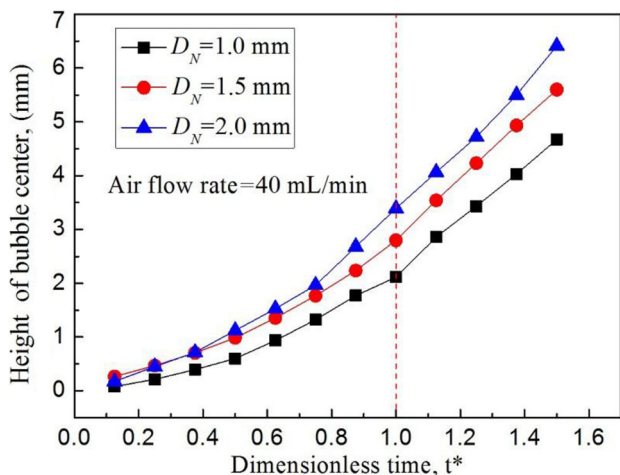
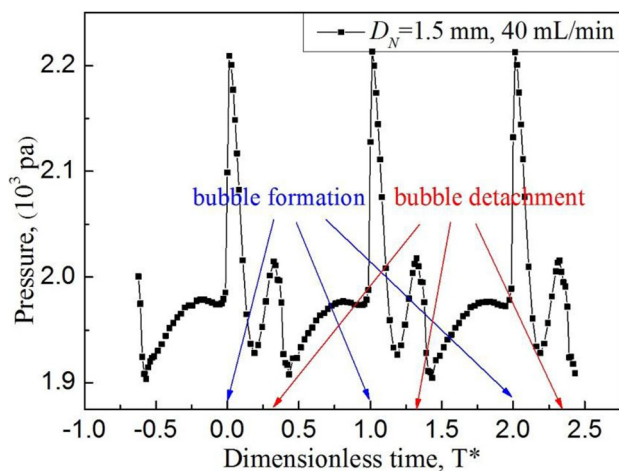


Fig. 7 (Color online) The height of bubble center at different dimensionless times

Table 2 Calculation results with an orifice diameter of 1.5 mm

Air flow rate (mL/min)	20			40			60		
	T (s)	t (s)	Volume ($\times 10^{-2}$ mL)	T (s)	t (s)	Volume ($\times 10^{-2}$ mL)	T (s)	t (s)	Volume ($\times 10^{-2}$ mL)
Experiment	0.114	0.032	3.80	0.074	0.030	4.93	0.068	0.029	6.80
Calculation	0.111	0.031	3.68	0.074	0.029	4.87	0.066	0.028	6.54
Error (%)	2.6	3.1	3.2	0	3.3	1.2	2.9	3.4	3.8

**Fig. 8** (Color online) Fluctuation of pressure at the wall orifice

increases rapidly, causing the pressure of the wall orifice to decrease rapidly. It can also be noted from the figure that there is a small pressure peak in the bubble formation process. The main reason behind this is the third stage of bubble formation, where the bubble starts to neck and the water phase gradually increases, such that the average pressure at the hole increases. In general, the bubble formation mechanism is controlled by the pressure fluctuation and this fluctuation at the orifice corresponds to the three stages of bubble formation.

4 Conclusion

In the present study, the dynamic behavior of bubbles formation and evolution from vertical wall orifice in quiescent pure water was investigated through visualization experiments and numerical simulations. To study the bubble formation, an orifice with diameter of 1.0, 1.5, and 2.0 mm and air flow rate of 20, 40, 60, 80, and 100 mL/min were used. The main conclusions of the study are as follows:

- (1) The evolution of the bubble formation process can be divided into three stages, namely nucleation, stable growth, and necking. In the first stage,

buoyancy is negligible and is mainly affected by surface tension. However, in the latter two stages, as the bubble volume increases, buoyancy plays an increasingly apparent role in bubble forming and deforming. The stage of necking is quite different from the bubble formation process by the bottom wall orifice.

- (2) A bubble can form only when the air-phase pressure exceeds the threshold pressure at wall orifice. Due to the influence of the threshold pressure and buoyancy, the bubble departure volume and formation period increase with a decrease in the wall orifice diameter. The results obtained were contrary to that of bubble formation from bottom wall orifice.
- (3) An agreement between the simulation and experimental results with the same condition is noted. The simulation results show that the pressure threshold and periodic pressure fluctuation at the orifice are related to the formation and shedding of bubbles. The pressure fluctuation at the orifice can directly reflect the three stages of bubble formation.

References

1. R.C. Robertson, MSRE design and operation report I, ORNL-0728. (U.S. Atomic Energy Commission, 1965), pp. 205–243
2. W.C. Tang, C.Q. Yan, L.C. Sun et al., Characteristic of bubble breakup in venturi-type bubble generator. *Atomic Energy Sci. Technol.* **48**(5), 843–847 (2014). <https://doi.org/10.7538/yzk.2014.48.05.0844>. (in Chinese)
3. X.F. Ju, L.C. Sun, W.C. Tang et al., Analysis of the operating characteristics of a Venturi-type bubble generator for MSR. *Nucl. Tech.* **37**(12), 120605 (2014). <https://doi.org/10.11889/j.0253-3219.2014.hjs.37.120605>. (in Chinese)
4. N. Kantarci, F. Borak, K.O. Ulgen, Bubble column reactors. *Process Biochem.* **40**, 2263–2283 (2005). <https://doi.org/10.1016/j.procbio.2004.10.004>
5. N. Yang, J.H. Chen, H. Zhao et al., Explorations on the multi-scale flow structure and stability condition in bubble columns. *Chem. Eng. Sci.* **62**, 6978–6991 (2007). <https://doi.org/10.1016/j.ces.2007.08.034>
6. G.Q. Yang, B. Du, L.S. Fan, Bubble formation and dynamics in gas-liquid-solid fluidization—a review. *Chem. Eng. Sci.* **62**, 2–27 (2007). <https://doi.org/10.1016/j.ces.2006.08.021>

7. N. Yang, Z.Y. Wu, J.H. Chen et al., Multi-scale analysis of gas-liquid interaction and CFD simulation of gas-liquid flow in bubble columns. *Chem. Eng. Sci.* **66**, 3212–3222 (2011). <https://doi.org/10.1016/j.ces.2011.02.029>
8. M. Pourtousi, J. Sahu, P. Ganesan, Effect of interfacial forces and turbulence models on predicting flow pattern inside the bubble column. *Chem. Eng. Process. Process Intensif.* **75**, 38–47 (2014). <https://doi.org/10.1016/j.cep.2013.11.001>
9. M. Pourtousi, J. Sahu, P. Ganesan, S. Shamshirband et al., A combination of computational fluid dynamics (CFD) and adaptive neuro-fuzzy system (ANFIS) for prediction of the bubble column hydrodynamics. *Powder Technol.* **274**, 466–481 (2015). <https://doi.org/10.1016/j.poetec.2015.01.038>
10. G.H. Yeoh, J. Tu, *Computational Techniques for Multiphase* (Butterworth-Heinemann, London, 2010), pp. 351–353
11. M. Pourtousi, P. Ganesan, A. Kazemzadeh et al., Methane bubble formation and dynamics in a rectangular bubble column: a CFD study. *Chemometr. Intell. Lab. Syst.* **147**, 111–120 (2015). <https://doi.org/10.1016/j.chemolab.2015.08.003>
12. M. Jamialahmadi, M.R. Zehtaban, H. Müller-Steinhagen et al., Study of bubble formation under constant flow conditions. *Chem. Eng. Res. Des.* **79**, 523–532 (2001). <https://doi.org/10.1205/02638760152424299>
13. X. Zhu, Q. Liao, H. Wang et al., Experimental Study of bubble growth and departure at the tip of capillary tubes with various wettabilities in a stagnant liquid. *J. Supercond. Novel Magn.* **23**(6), 1141–1145 (2010). <https://doi.org/10.1007/s10948-010-0723-y>
14. L. Zhang, M. Shoji, Aperiodic bubble formation from a submerged orifice. *Chem. Eng. Sci.* **56**(18), 5371–5381 (2001). [https://doi.org/10.1016/S0009-2509\(01\)00241-X](https://doi.org/10.1016/S0009-2509(01)00241-X)
15. V.V. Buwa, D. Derlach, F. Durst et al., Numerical simulation of bubble formation on submerged orifice: period-1 and period-2 bubbling regimes. *Chem. Eng. Sci.* **62**(24), 7119–7132 (2007). <https://doi.org/10.1016/j.ces.2007.08.061>
16. A. Bhunia, S.C. Pais, Y. Kamotan et al., Bubble formation in a coflow normal and reduced configuration in gravity. *AIChE J.* **44**(7), 1499–1509 (1998). <https://doi.org/10.1002/aic.690440704>
17. H.K. Nagra, Y. Kamotani, Bubble formation from wall orifice in liquid cross-flow under low gravity. *Chem. Eng. Sci.* **55**, 4653–4665 (2000). [https://doi.org/10.1016/S0009-2509\(00\)00102-0](https://doi.org/10.1016/S0009-2509(00)00102-0)
18. H.K. Nagra, Y. Kamotani, Prediction of bubble diameter at detachment from a wall orifice in liquid cross-flow under reduced and normal gravity conditions. *Chem. Eng. Sci.* **58**, 55–69 (2003). [https://doi.org/10.1016/S0009-2509\(02\)00516-X](https://doi.org/10.1016/S0009-2509(02)00516-X)
19. I. Chakraborty, G. Biswas, P.S. Ghoshdastidar, A coupled level-set and volume-of-fluid method for the buoyant rise of gas bubbles in liquids. *Int. J. Heat Mass Transfer.* **58**, 240–259 (2013). <https://doi.org/10.1016/j.ijheatmasstransfer.2012.02.053>
20. J. Xie, X. Zhu, Q. Liao et al., Dynamics of bubble formation and detachment from an immersed micro-orifice on a plate. *Int. J. Heat Mass Transfer.* **55**, 3205–3213 (2012). <https://doi.org/10.1016/j.ijheatmasstransfer.2012.11.027>
21. J. Zhang, Y. Yu, C. Qu et al., Experimental study and numerical simulation of periodic bubble formation at submerged micron-sized nozzles with constant gas flow rate. *Chem. Eng. Sci.* **168**, 1–10 (2017). <https://doi.org/10.1016/j.ces.2017.04.012>
22. Y.J. Zhang, M.Y. Liu, Y.G. Xu et al., Three-dimensional volume of fluid simulations on bubble formation and dynamics in bubble columns. *Chem. Eng. Sci.* **73**, 55–78 (2012). <https://doi.org/10.1016/j.ces.2012.01.012>
23. K. Mukundakrishnan, S. Quan, D.M. Eckmann et al., Numerical study of wall effects on buoyant gas-bubble rise in a liquid-filled finite cylinder. *Phys. Rev. E* **76**, 036308–01–15 (2007). <https://doi.org/10.1103/PhysRevE.76.036308>
24. K.Y. Zhang, Y.Q. Feng, P. Schwarz et al., Computational fluid dynamics (CFD) modeling of bubble dynamics in the aluminum smelting process. *Ind. Eng. Chem. Res.* **52**(33), 11378–11390 (2013). <https://doi.org/10.1021/ie303464a>
25. Z.B. Zhao, Y.Q. Feng, P. Schwarz et al., Numerical modeling of flow dynamics in the aluminum smelting process: comparison between air-Water and CO₂-cryolite systems. *Metall. Mater. Trans. B* **48**, 1200–1216 (2017). <https://doi.org/10.1007/s11663-016-0872-x>
26. K.B. Cai, Y.C. Song, J.J. Li et al., Pressure and velocity fluctuation in the numerical simulation of bubble detachment in a Venturi-type bubble generator. *Nucl. Technol.* **205**, 94–103 (2018). <https://doi.org/10.1080/00295450.2018.1479575>
27. D. Ma, M.Y. Liu, Y.G. Zu et al., Two-dimensional volume of fluid simulation studies on single bubble formation and dynamics in bubble columns. *Chem. Eng. Sci.* **72**, 61–77 (2012). <https://doi.org/10.1016/j.ces.2012.01.013>
28. W. Helden, C. Geld, P. Boot, Forces on bubbles growing and detaching in flow along a vertical wall. *Int. J. Heat Mass Transfer.* **38**(11), 2075–2088 (1995). [https://doi.org/10.1016/0017-9310\(94\)00319-Q](https://doi.org/10.1016/0017-9310(94)00319-Q)
29. J.F. Klausner, R. Mei, D.M. Bernhard et al., Vapor bubble departure in forced convection boiling. *Int. J. Heat Mass Transfer.* **36**(3), 651–662 (1993). [https://doi.org/10.1016/0017-9310\(93\)80041-r](https://doi.org/10.1016/0017-9310(93)80041-r)